ELECTROMAGNETIC SHIELDING PROPERTIES OF IRON OXIDE IMPREGNATED KENAF BAST FIBERBOARD

Zhiguang Ding

Thesis Prepared for the Degree of

MASTER OF SCIENCE

UNIVERSITY OF NORTH TEXAS

December 2014

APPROVED:

Sheldon Shi, Major Professor
Xiaohua Li, Committee Member
Hualiang Zhang, Committee Member
Yong Tao, Chair of the Department of Mechanical and Energy Engineering
Costas Tsatsoulis, Dean of the College of Engineering
Mark Wardell, Dean of the Toulouse Graduate School

Ding, Zhiguang. *Electromagnetic Shielding Properties of Iron Oxide Impregnated Kenaf Bast Fiberboard*. Master of Science (Mechanical and Energy Engineering), December 2014, 27 pp., 6 tables, 8 figures, references, 19 titles.

The electromagnetic shielding effectiveness of kenaf bast fiber based composites with different iron oxide impregnation levels was investigated. The kenaf fibers were retted to remove the lignin and extractives from the pores in fibers, and then magnetized. Using the unsaturated polyester and the magnetized fibers, kenaf fiber based composites were manufactured by compression molding process. The transmission energies of the composites were characterized when the composite samples were exposed under the irradiation of electromagnetic (EM) wave with a changing frequency from 9 GHz to 11 GHz. Using the scanning electron microscope (SEM), the iron oxide nanoparticles were observed on the surfaces and inside the micropore structures of single fibers. The SEM images revealed that the composite's EM shielding effectiveness was increased due to the adhesion of the iron oxide crystals to the kenaf fiber surfaces. As the Fe content increased from 0% to 6.8%, 15.9% and 18.0%, the total surface free energy of kenaf fibers with magnetizing treat increased from 44.77 mJ/m^2 to 46.07 mJ/m^2, 48.78 mJ/m^2 and 53.02 mJ/m^2, respectively, while the modulus of elasticity (MOE) reduced from 2,875 MPa to 2,729 MPa, 2,487 MPa and 2,007 MPa, respectively. Meanwhile, the shielding effectiveness was increased from 30-50% to 60-70%, 65-75% and 70-80%, respectively.

ACKNOWLEDGEMENTS

This thesis has been made possible by two important groups of people in my life.

Primarily, I would like to acknowledge the highest gratitude to my adviser, Dr. Sheldon Shi, who supported my whole Master's graduate study. He guided me and helped me a lot in biomaterial research. It has been my honor to be his student.

I would like to acknowledge, Dr. Hualiang Zhang and her team guide me a lot in the measurement of EM shielding effectiveness.

Appreciation is also extended to my parents for raising me up and giving me this chance to study aboard. Thanks my lab mate Changlei Xia, who always help and guide me in our lab, and Dr. Liping Cai, for his unconditional support and help.

TABLE OF CONTENTS

Page

LIST OF TABLES

Page

LIST OF FIGURES

Page

CHAPTER 1

INTRODUCTION

Electromagnetic (EM) pollution is from EM emitting radiations, which has become worldwide preoccupation (Huynen et al. 2011) because it is potentially harmful to human health. Driven by the proliferation of electronics and instrumentation in commercial and industrial applications, shielding by EM absorption has received arising interest in many areas. This is a serious issue caused by the interference effects of current induced by electric and magnetic fields (Saini et al. 2008). The interference among business machines, process equipment, consumer products and other instruments may lead to disturbance of usual performance or even complete malfunction. The disturbances across the communication channels, automation and process control may lead to loss of valuable time, energy, resources, money or even precious human life. Therefore, the shielding mechanism must be provided to understand the spurious electromagnetic noises or pollution.

In order to reduce the EM field in a space, the EM shielding technique is developed to block the field with barriers made of conductive or magnetic materials. Using this EM shielding technique, the energy of EM wave is reduced to avoid the interference to the working electronic components (Koh et al. 2013, Li et al. 2013). At the present time, EM shielding and microwave energy absorbing materials have been designed and synthesized to reduce the fault probability of electronic equipment caused by the EM noises and pollution.

It is well known that, because of its good mechanical properties and electric conductivity, metal is the most common EM shielding material and is extensively used in EM shielding

applications (Hou et al. 2013, Wang et al. 2006). Using the shielded cable as an example, an inner core conductor is surrounded by a wire mesh. The shielding prevents the signals transmitted by the inner conductor, stops them from leaking or being disturbed. The microwave oven has a door with a build-in metal screen. This screen isolates the oven's metal housing, stops the crossing EM wave, and allows the visible light to pass through.

However, as a good EM waver reflector but bad absorber due to their shallow skin depth (Li et al. 2005), metal also shows the disadvantages, such as high density, corrosive and uneconomic processing. These weaknesses hindered them for the practical applications in the EM signal shielding field. Therefore, it is beneficial to develop new materials which can perform similar EM shielding character with metal, but more easy-manufactured, economical and portable.

Due to the outstanding properties such as environmental-friendly and easy-processing, natural fiber is considered a good choice to be used in the EM shielding filed after magnetization or carbonization. Many wooden materials with different shielding levels have been tested and reported. In 1999, Nagasawa et al. (1999) investigated the production of wooden materials with effective electromagnetic shielding properties. Wood particles metallized by electroless plating were suitable as a raw material for the manufacture of particleboards. The specific gravity of the particleboard was about half of that for the plastic composite materials. Nagasawa's group observed a correlation between the surface and volume resistivity of the metallized wood particles, and the shielding effectiveness of the particleboard. The shielding effectiveness of the particleboard was improved by increasing the quantity of metallized wood particles and the applied pressure.

Wang et al. (2006) prepared the electrical and EM shielding wood-metal composite by applying the electroless nickel planting method. Electroless plating process method was used to prepare the lightweight wood veneers with Ni-P alloy surface-coated. NaH_2PO_4-water solution was used as the reductant in plating solution. Ni particles deposited on the fiber surface and formed continuous wood layers with electro-conductivity and EM shielding effectiveness. The result showed that the higher the plating solution amount, the higher the plating temperature, and the longer the reacting time affect the EM shielding effectiveness of sample in a positive way.

Saini et al. (2009) created highly conducting polyaniline (PANI)-multi-walled carbon nanotube (MWCNT) nanocomposites *in situ* polymerization. The results from Fourier transform infrared spectroscopy (FTIR) and X-ray diffraction (XRD) showed the systematic shifting of the characteristic bands and peaks of PANI, with an increase in MWCNT phase, suggesting a significant interaction between the phases. The scanning electron microscope (SEM) and transmission electron microscope (TEM) pictures show thick and uniform coating of PANI over surface of individual MWCNT. Based on the observed morphological features in SEM, the probable formation mechanism of these composites was proposed. The electrical conductivity of PANI–MWCNT composite (19.7 S cm^{-1}) was better than MWCNT (19.1 S cm^{-1}) or PANI (2.0 S cm^{-1}). This could be ascribed to the synergistic effect of two complementing phases (i.e. PANI and MWCNT). The absorption dominated total shielding effectiveness of −27.5 to −39.2 dB of these composites indicating the usefulness of these materials for microwave shielding in the Ku-band (12.4–18.0 GHz). These PANI coated MWCNTs with large aspect ratio were also proposed as the hybrid conductive fillers in various thermoplastic matrices, for making structurally strong

microwave shields.

The electromagnetic interference (EMI) shielding mechanisms of multi-walled carbon nanotube (MWCNT)/polymer composites were analyzed experimentally and theoretically by Al-Saleh and Sundararaj (2009). For the experimental analysis, EMI shielding effectiveness of MWCNT/ polypropylene (PP) composite plates were studied. A model based on the shielding of EM plane wave was used to theoretically study the EMI shielding mechanisms. The experimental results showed that the energy absorption was the major shielding mechanism and reflection was the secondary shielding mechanism. The modeling results demonstrated that multiple-reflection within the MWCNT internal surfaces and between the MWCNT external surfaces decreased the overall EMI shielding effectiveness. The EMI shielding effectiveness of MWCNT/PP composites increased with as the MWCNT content and shielding plate thickness increased.

In order to allow electronic components to coexist without harmful EMI, it is necessary to develop effective shielding and absorbing materials with high performance in reducing the transmitted energy and a large operating frequency band (Lakshmi et al. 2009). It was found that the conducting polymer composites were suitable for the EMI shielding and the dissipation of electrostatic charge. The microwave absorption, microwave reflection and EMI shielding properties of PANI–PU composite is evaluated both at S-band and X-band frequencies. It was confirmed that the material had good microwave absorption and potential to be used for EMI shielding.

In the later study of Saini et al. (2011), blends of polystyrene with polyaniline (PANI) coated multi-walled carbon nanotubes (MWCNTs) were designed for inherit dielectric and

magnetic attributes from PANI and MWCNT. The high resolution TEM image showed that the PANI coating over MWCNT containing entrapped Fe catalyst. These blends showed that the absorption dominated total shielding effectiveness (SET) of −45.7 dB (>99.99% attenuation) in the 12.4–18.0 GHz range, suggesting their utility for making efficient microwave absorbers. The enhanced SET was ascribed to optimization of conductivity, skin-depth, complex permittivity and permeability. A good agreement between the theoretical prediction and the experimental shielding measurements was also observed.

To improve the EM shielding, especially the energy absorption of carbon fiber reinforced polymer–matrix composites for aircraft applications in high frequencies, Jalalia et al. (2011) used the metallic nanoparticles of iron, cobalt, nickel and iron oxide as a filler into the carbon fiber/polymer. It was found that the iron nanoparticles of 50 nm were able to improve the total shielding effectiveness of a carbon fiber/polymer nanocomposite up to 15 dB in the considered 8.2–12.4 GHz ranging band. At the same time, the EM shielding behavior was a superiorly constant; while the absorption part of shielding was increased.

Jin Heon Kwon's group (2012) developed a new method to incorporate the natural fibers into the EM shielding area. Instead of introducing metal particles into the specimen, the fibers were carbonized themselves to decrease the electric resistance. Using the technique, a series of medium density fiberboard (MDF) were manufactured. Kwon's group carbonized the MDF specimens at 700ºC and found them has stable and low EM interference values (1.3-7.6 dB) between 10MHz and 1GHz frequency. The MDF specimen carbonized at 800 ºC performed a good EM interference (43.1dB for average) and could meet the industrial requirement. However, when

the MDF was carbonized at above 900-1,500 ºC, high EM interference values (66.8-84.6 dB) of the board were obtained. The increase from 600 ºC to 700 ºC of the carbonizing temperature caused a significant decrease for the electrical resistivity (from 180,900 to 137.5 Ω/cm). However, when the carbonization temperature varied from 1,300 ºC to 1,500 ºC, the electrical resistivity did not change very much. The treatment also lowered the modulus of rupture, but increased the modulus of elasticity.

Bollen et al. (2013) developed a sandwich structure involving a honeycomb core filled with a carbon nanotube-reinforced polymer foam and glass fiber-reinforced composite face sheets to combine high electromagnetic absorption and high mechanical performance. The large electromagnetic absorption is attained by simultaneously minimizing the reflection and transmission. The sandwich also offers high stiffness versus density performance.

Although scientists have been using the natural fibers in the EM shielding field, no technique has been reported to use iron oxide impregnated fiberboard to shield EM signals. It is known that iron oxide performs excellent magnetic property and the iron oxide impregnated fiber based composites will shield EM signal effectively. In this study, the iron oxide impregnated kenaf fiber composites for the EM shielding was fabricated. The kenaf fibers used in this method were retted by 5% NaOH-water solution for removing the lignin to create void space of the fibers so that a high iron oxide nanoparticle loading could be obtained.

CHAPTER 2

MATERIALS AND METHODS

All reagents and solvents used in the experiments were analytical grade and without any further purification. Kenaf fibers are supplied by Kengro Corporation, Charleston, MS. Ferrous chloride tetrahydrate ($FeCl_2.4H_2O$) and Ferric chloride hexahydrate ($FeCl_3.6H_2O$) with above 99.95% purity were purchased by Fisher Science Education. Ammonium hydroxide water solution with 28-30wt% was purchased by Acros Organics. Polyester AROPOL Q 6585 with 30-40% Styrene and Tert-Butl peroxybenzoate with 98% purity were supplied by Ashland Chemical Company.

2.1 Fiber Retting

Kenaf fibers of 100g with a moisture content of 11% were added into 2,000g water solution with 5% NaOH in a sealed reactor. The mixture was treated at 160ºC for 14 hours. The fibers were washed with distilled water for up to 20 times to reach the pH value of 7. Then the fibers were dried to 0% moisture content in the oven at 373.1K for 14 hours.

2.2 Fiber Magnetization

The reaction follows the equation:

$$2FeCl_3 + FeCl_2 + 8NH_3 + 4H_2O \implies Fe_3O_4 + 8NH_4Cl$$

A mixture of 2,000g FeCl3 and FeCl2 water solutions was mechanically stirred at a constant speed of 120 rpm of 120 minutes under the ambient pressure and temperature. Thirty

grams of retted kenaf fibers were added into the solution. After 14 hours of soaking, the fibers were uniformly absorbed with the ferric and ferrous ion solution. Then the NH_3 solution was dropped slowly into the mixture with stirring. The iron oxide nanoparticles were formed inside the micropore structures of the fibers.

After the NH_3 solution was added in, the mixture was kept stirring for 8-10 hours and then remained overnight. After the liquid mixture was poured onto a 1mm x 1mm screen metal mash for filtering and washed with distilled water until the pH value=7, it was dried at 120 ºC for 10-12 hours. Figure 2.1 shows the change of appearance on the kenaf fibers before and after the magnetizing treatment.

Figure 2.1. Kenaf fibers before and after the magnetizing treatment.

By adjusting the ion concentration of $FeCl_3$ and $FeCl_2$ water solutions according to Table 2.1, the desired amount of iron oxide in the mixture as the resultant of the reaction was obtained. Using this method, three different magnetizing levels of kenaf fibers were obtained.

Table 2.1

The Ion Concentrations for Fe^{3+} and Fe^{2+} in Magnetizing Water Solutions

Sample	Ion concentration of Fe^{3+}	Ion concentration of Fe^{2+}
0	Control Sample	Control Sample
1	1mol/L	0.5mol/L
2	2mol/L	1mol/L
3	4mol/L	2mol/L

2.3 Board Manufacturing

Using the magnetized fibers, four kenaf fiber based composites with different levels of iron oxide magnetization were manufactured to examine the effect of EM shielding and the mechanical properties of the composites. The unsaturated polyester AROPOL Q 6585 and Tert-Butl peroxybenzoate were used as resin and catalyst, respectively. A mixture of 20 g of resin and 1g of catalyst were added to the 30g well-magnetized kenaf fiber, resulting in a perform mat. The mat was placed in a hot-press with a pressure of 100 psi. The resin curing process was completed in the hot-press with the pre-curing at 100 ºC for 2 hours and curing at 150 ºC for 2 hours. The Carver hot press (model 3693) was used to manufacture the fiberboard specimens. The dimensions of the specimens are: 83.2 mm x 56.3 mm x 6.4 mm.

2.4 Characterizations

2.4.1 Surface Morphology of Kenaf Fibers

The surface morphology of untreated and treated kenaf fibers was characterized by the dual column ultra-high resolution field emission scanning electron microscope (SEM, S-4800, Hitachi,

Japan). The detailed specifications for Hitachi Model S-4800, field emission scanning electron microscope are shown in reference.

2.4.2 Surface Free Energy Measurement of Kenaf Fibers

The fiber diameters and contact angles were measured by the Dynamic Contact Angle analyzer model DCA-322 (Thermo Scientific Instrument). DCA-322 offers powerful and versatile approaches to the comprehensive understanding of the complex interactions at liquid-liquid and liquid-solid surfaces. The detailed specification of DCA 322 is shown in reference.

The surface free energies of samples were calculated by the collected data and the Wilhelmy equation:

$$F \times g = \gamma \times \pi \times \text{Diameter} \times \cos\theta,$$

$\cos\theta$ can be obtained only if the other parameters are known or measured. Therefore, with this method, it's necessary to have the g,γ and dimension of the solid probe entered into the software correctly. The recommended steps for these three methods are shown in Table 2.2.

Table 2.2

Recommended Steps for Three Methods of Determining Surface Free Energy

Single Cycle and Single Loop (default method)	Single Cycle and Multiple Loops	Multiple Cycles and Multiple Loops
Set Speed Tare Balance Detect ZDOI Advance Dwell (optional) Recede Return to Zero Position	Same as the Single Cycle and Single Loop method, but with more than one advance/recede loops before the "Return to Zero Position" step	different cycles which can be a combination of the previous two methods

An exemplary contact angle run of a piece of polymer against distilled water is demonstrated in Figure 2.2, by using the default single cycle single loop method. It is obvious in the Figure that advancing and receding traces have a negative slope in them due to the increasing of the buoyancy force, as the solid enters the liquid deeper. The data range is shown by the boxes on the advancing and receding parts of the curves, which are used for linear regression to perform line fit and extrapolation to "eliminate" buoyancy force. The calculated results for advancing and receding are shown in the upper left corner, in the order of $\cos\theta$, θ, and regression factor.

It is necessary to mention that the range of data that are used for calculation can be modified in the software.

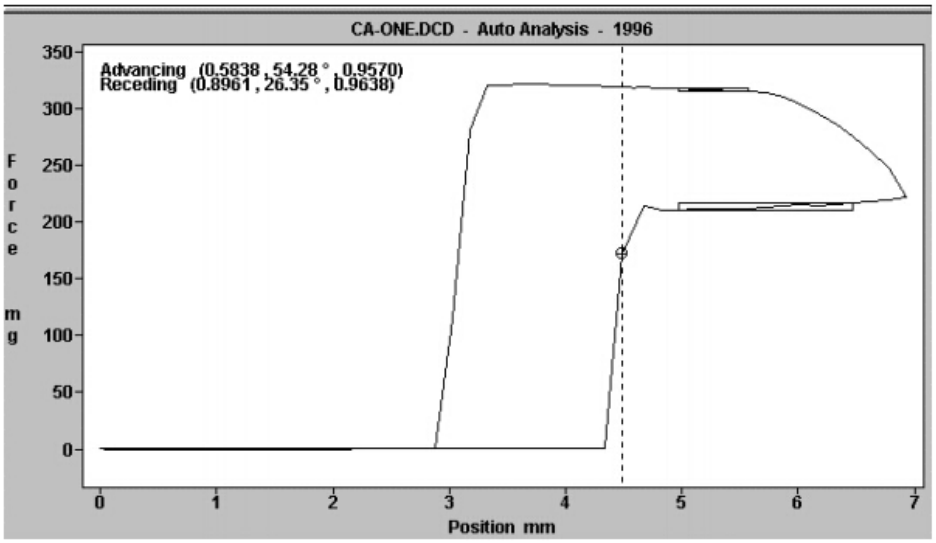

Figure 2.2. An exemplary contact angle run on DCA-322 of a piece of polymer against distilled water.

For fiber sample with a very small diameter, about a few micrometers, it's very difficult to measure an accurate value of diameter. Even though an optical microscope can be applied aiming this purpose, it is still time-consuming and difficult to control the sample and the device manually. Moreover, the result obtained from this method varies with the measuring direction and the

measuring point within one single fiber.

DCA method is very simple and the measurement is quick comparing to the traditional measuring method, such as optical microscope. Also an accurate averaged diameter can be obtained. The fiber diameter is contained in the Wilhelmy Equation:

$$F \times g = \gamma \times \pi \times \text{Diameter} \times \cos\theta$$

By applying a very low surface tension liquid to make contact angle 0°, or $\cos\theta = 1$, the fiber diameter can be obtained as:

$$\text{Diameter} = F \times \frac{g}{\gamma \times \pi}$$

In the diameter measurement, Hexane is used as probe liquid to ensure the total wetting angle, or 0°, or $\cos\theta = 1$ is obtained.

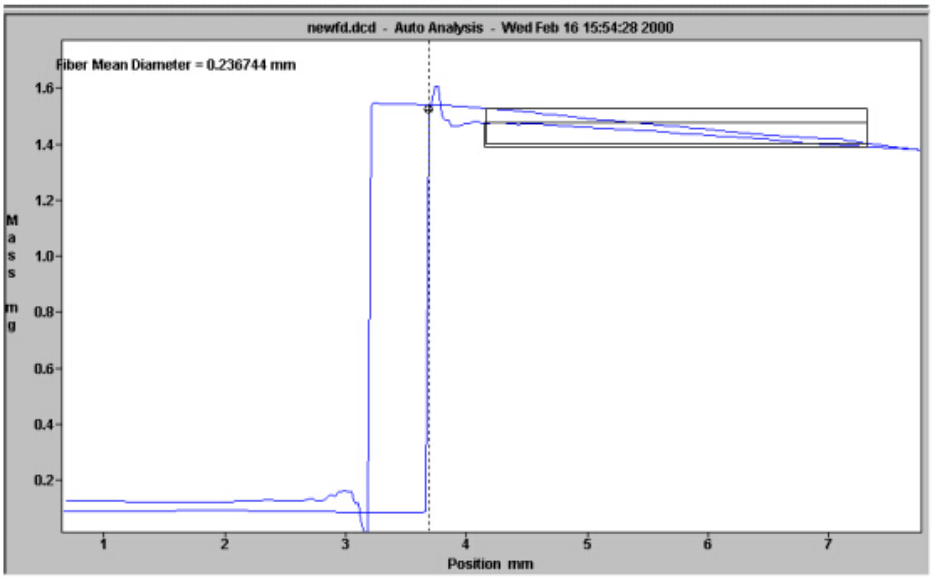

Figure 2.3. A typical fiber diameter run on DCA-322.

The experimental progresses of the contact angle measurement by DCA are similar as those of the contact angle sampling technique, with single cycle single loop. Since most of the low surface tension liquids are volatile, there is a possibility that liquid vapor is absorbed into the

sample during the testing. Therefore, only the advancing data is used for calculating the fiber's diameter. A typical fiber diameter run is illustrated as follows in Figure 2.3.

For fiber diameter and contact angle, each test was repeated 5 times and the average value was used for calculation.

2.4.3 The Modulus of Elastic Measurement of Magnetized Kenaf Fiberboard

The Modulus of Elastic (MOE) of fiberboards was measured using the Universal Testing Machine (Shimadzu Corporation AutoGraph AGS-X Series, Japan). The detailed specifications are shown on the following website of Shimadzu Company:

http://www.shimadzu.com/an/test/universal/ags-x/ags-x_6.html

Figure 2.4. Universal testing machine for the measurement of the mechanical property measurement.

This machine was operated under 5 kN mode. The Modulus of Elastics of material was determined in this test on a specimen with a dimension of 83.2 mm by 8 mm by 6.4 mm. The failure mode of the test was set at 50% of the peak load. Testing speed was 1 mm/min. Five replicates were conducted for each sample type.

2.4.4 The EM Shielding Effectiveness Measurement

Network analyzer is an instrument that measures the network parameters of electrical networks. Network analyzers commonly measure s–parameters because that the reflection and transmission of electrical networks are easy to measure at high frequencies.

Vector network analyzer (VNA) measures both amplitude and phase properties. VNA is the most common type of network analyzers. A VNA may also be called a gain-phase meter or an automatic network analyzer.

The basic architecture of a network analyzer involves a signal generator, a test set, one or more receivers and display. Most VNAs have two test ports, permitting measurement of four S-parameters (S11, S21, S12 and S22). The instruments with more than two ports are available commercially.

The network analyzer needs a test signal, and a signal generator or signal source can provide one. Nearly all modern network analyzers have a built-in signal generator. High-performance network analyzers have two built-in sources.

The test set takes the signal generator output and routes it to the device under test, and it routes the signal to be measured to the receivers. It often splits off a reference channel for the incident wave. In a VNA, the reference channel goes to the receivers; it is needed to serve as a phase reference.

The receivers make the measurements. A network analyzer will have one or more receivers connected to its test ports. The reference test port is usually labeled R, and the primary test ports are A, B, C and so on. Some analyzers will dedicate a separate receiver to each test port, but others

share one or two receivers among the ports. The R receiver may be less sensitive than the receivers used on the test ports.

For the VNA, the receiver measures both the magnitude and the phase of the signal. It needs a reference channel (R) to determine the phase, so a VNA needs at least two receivers. The usual method converts the reference and test channels to make the measurements at a lower frequency. The phase may be measured with a quadrature detector. A VNA requires at least two receivers, but some will have three or four receivers to permit simultaneous measurement of different parameters.

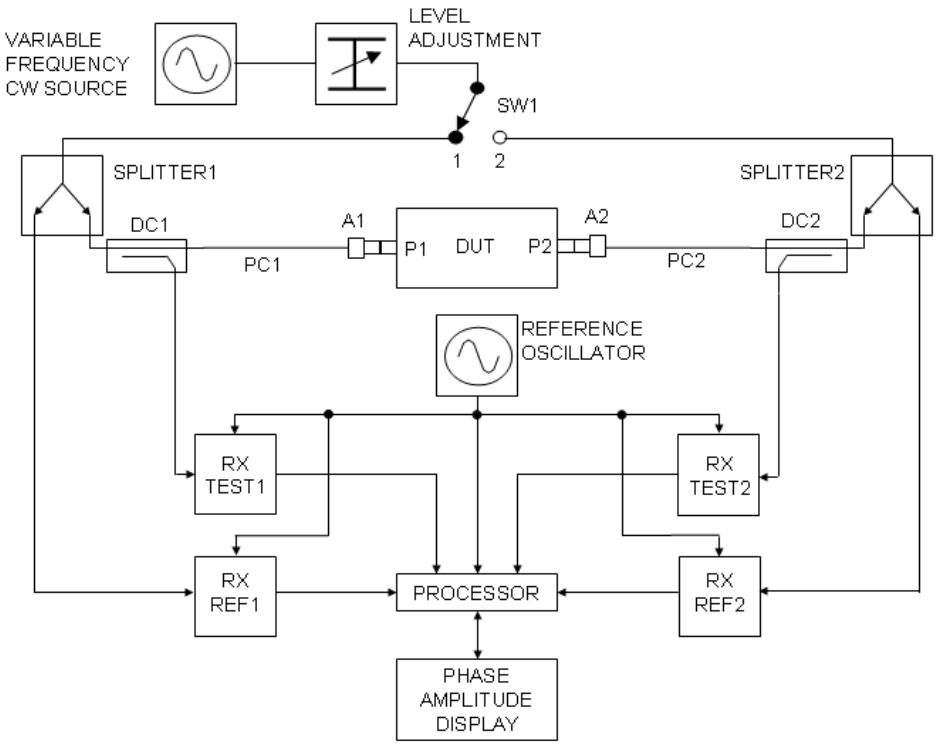

Figure 2.5. The basic parts of a vector network analyzer (from Wikipedia).

The diagram shows the essential parts of a typical 2-port VNA. The two ports of the device under test (DUT) are denoted port 1 (P1) and port 2 (P2). The test port connectors on the VNA are

precision types which will normally have to be extended and connected to P1 and P2 using precision cables 1 and 2, PC1 and PC2 respectively and suitable connector adaptors A1 and A2, respectively.

The test frequency is generated by a variable frequency continues-wave source and its power level is set using a variable attenuator. The position of switch SW1 sets the direction that the test signal passes through the DUT. Initially, the SW1 is considered at position 1 so that the test signal is an incident on the DUT at P1 which is appropriate for measuring S11 and S21. The test signal is fed by SW1 to the common port of splitter 1, one arm (the reference channel) feeding a reference receiver for P1 (RX REF1) and the other (the test channel) connecting to P1 via the directional coupler DC1, PC1 and A1. The third port of DC1 couples off the power reflected from P1 via A1 and PC1, then feeding it to test receiver 1 (RX TEST1). Similarly, the signals leaving P2 pass via A2, PC2 and DC2 to RX TEST2. RX REF1, RX TEST1, RX REF2 and RXTEST2 are known as coherent receivers as they share the same reference oscillator, and they are capable of measuring the test signal's amplitude and phase at the test frequency. All of the complex receiver output signals are fed to a processor which does the mathematical processing and displays the chosen parameters and format on the phase and amplitude display. The instantaneous value of phase includes both the temporal and spatial parts, but the former is removed by virtue of using 2 test channels: one is for a reference and the other is for the measurement. When SW1 is set to position 2, the test signals are applied to P2, the reference is measured by RX REF2, reflections from P2 are coupled off by DC2, measured by RX TEST2, and the signals leaving P1 are coupled off by DC1 and measured by RX TEST1. This position is

appropriate for measuring S22 and S12.

In the work of this research, the EM shielding effectiveness of the magnetized board was measured using the Vector Network Analyzer (VNA, ZVB-20, Rohde&Schwarz, Germany). WR-90 to SMA Female Connector Waveguide to Coax Adapter from 8.2 GHz to 12.4 GHz, provided by Fairview Microwave, Inc., was selected and applied as the waveguide. The effectiveness values were measured from the central areas of kenaf fiberboards. The scanning speed with the frequency increasing from 9 GHz to 11 GHz is 0.5 GHz/s. Then the scanning process was repeated automatically by VNA. When the waveform was stable, the data was collected and used for further analyzing.

Figure 2.6. Vector Network Analyzer for the measurement of EM shielding effectiveness.

CHAPTER 3

RESULTS AND DISCUSSION

3.1 Iron Content of the Magnetized Kenaf Fibers

Each sample, 30g retted kenaf fiber was magnetized with different concentrations of iron oxide. The iron contents of fibers after the magnetizing were estimated from the weight changes of the fibers before and after the treatments. The weight changes and the calculated iron contents are presented in the Table 3.1.

Table 3.1

The Weight Changes and Calculated Iron Contents in the Progress of Magnetizing

Sample	Weight		Iron oxide Weight	Iron Content
	Before treatment	After Treatment		
0	30.00g	30.00g	0.00g	0.0%
1	30.00g	33.10g	3.10g	6.8%
2	30.00g	36.52g	6.52g	15.9%
3	30.00g	39.94g	9.94g	18.0%

3.2 Surface Morphology of the Untreated and Treated Kenaf Fibers

Microstructure and morphology were investigated through SEM observation. The surface morphology of the untreated fibers (A) shows relatively smoothy surfaces and unexpended diameters. Images (B), (C) and (D) distinctly demonstrate the gradual expansion of fiber diameters, the continuous crystallization of iron oxide on fiber surfaces, and the gaps between fibers. The iron

oxide nanoparticles are observed mainly inside the fibers and attached to the fiber surface as shown in Fig.3.1(C). As the Fe content increased, the iron oxide nanoparticles were found in the gaps among the fibers.

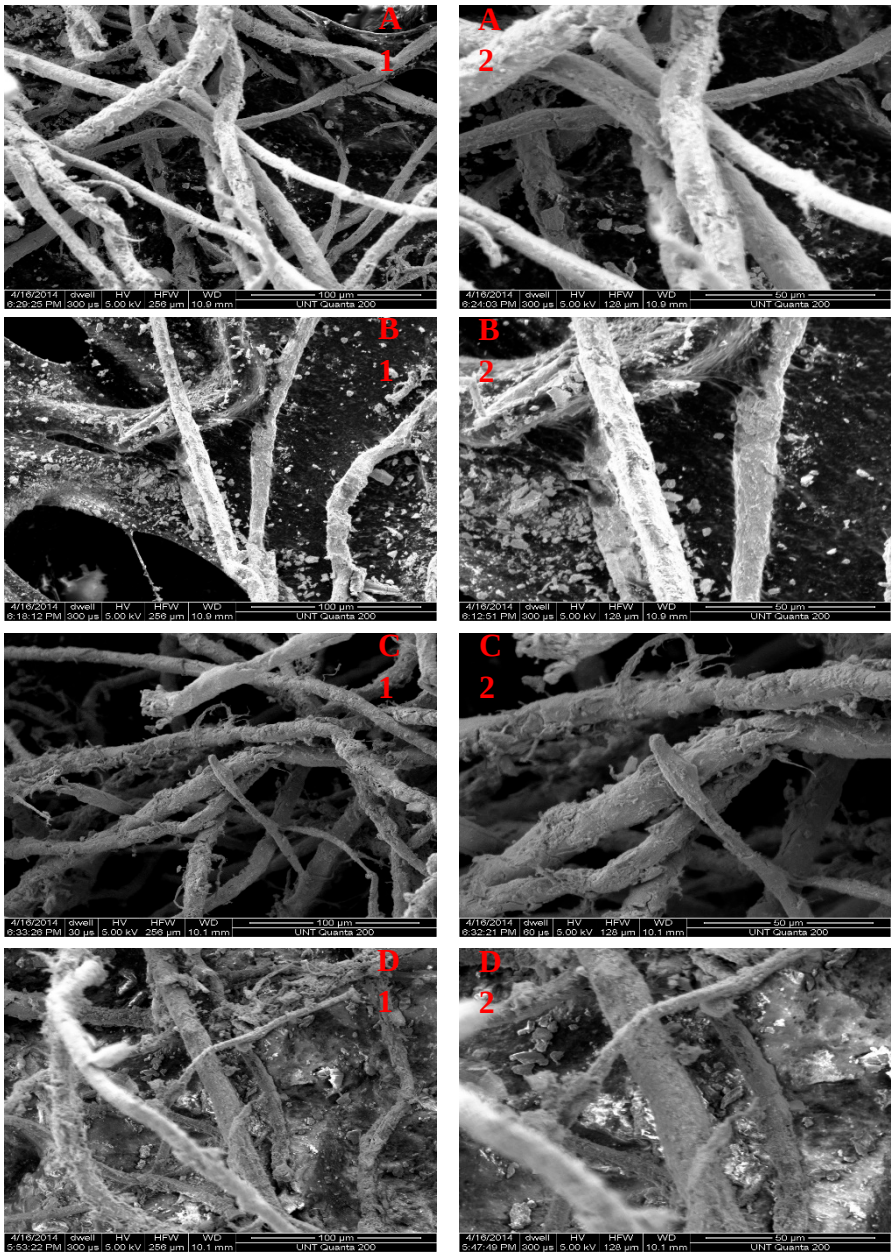

Figure 3.1. SEM morphologies of kenaf fibers magnetized with different level treatment: (A) Sample No. 0, Fe content=0%, (B) Sample No. 1, Fe content=6.8%, (C) Sample No. 2, Fe content=15.9%, (D) Sample No. 3, Fe content=18.0%.

3.3 Contact Angles and Surface Free Energy of Magnetized Kenaf Fibers

The Dynamic Contact Angle analyzer model DCA-322 manufactured by Thermo Scientific Instrument of Germany was used for the dynamic contact angle measurements. A Microsoft-Windows' based computer with the Win DCA software program installed was interfaced to the DCA-322 equipment for data analysis and display.

DCA-322 is commonly used to measure the diameter of a single fiber. The following steps are applied on the samples in order to complete the measurement successfully and efficiently:

i. A set of metal wire support was prepared and bent into "7" shape, and one end was attached to the balance loop, and the other straight end was attached to the fiber.

ii. The single fiber sample was mounted onto the metal wire support by small pieces of tape, which prevented from the absorption of the probe liquid. A very short piece of fiber sample (about 2 to 4mm) was exposed to gain rigidity.

iii. Hexane (nonpolar with low surface tension) was selected to be the probe liquid. During the data collection, a stage moving speed of 80mm/min was used. By raising the elevating platform at a constant speed, the fiber sample was immersed into the testing liquid.

iv. After calibration the test procedure was started. The results were shown by software when the measurement was completed. The reported diameters were the average of five measurements.

The next step is the measurement of contact angle of fibers and testing liquids. Sample installation and stage moving speed were the same as the diameter measurement. Using two liquids, water and formamide, the contact angle values were collected and used to determine the surface energy of the fibers. The reported contact angles were the average of five measurements.

The fiber diameters and dynamic contact angles (θ) were obtained as shown in Table 3.2.

Table 3.2

Contact Angles of Kenaf Fibers Before and After Magnetization Treatments

Sample		Diameter of Fibers (mm)		Testing Liquid: Water (Advanced)		Testing Liquid: Formamide (Advanced)	
	Fe Content	Average	St. Div.	Average	St. Div.	Average	St. Div.
#0	0%	0.093	0.015	58.37°	5.51°	42.41°	1.39°
#1	6.78%	0.116	0.021	60.26°	2.55°	38.63°	3.41°
#2	15.87%	0.120	0.020	69.53°	2.32°	37.78°	3.46°
#3	18.02%	0.124	0.019	70.64°	2.55°	33.85°	2.10°

The surface free energy of fibers was calculated according to the equations (1) and (2)

$$\gamma_l(1+\cos\theta) = 2\sqrt{\gamma_s^p \gamma_l^p} + 2\sqrt{\gamma_s^d \gamma_l^d} \quad (1)$$

$$\gamma_{total} = \gamma_s^p + \gamma_s^d \quad (2)$$

where θ is the dynamic contact angle between the fiber and the testing liquid, which was calculated by the computer program, γ_l is the surface tension of the testing liquid; γ_{total}, γ_s^p and γ_s^d are the total surface free energy of the fiber sample, the polar component and the dispersive component of total surface free energy, respectively. γ_l^p and γ_l^d are the polar component and the dispersive component of total surface free energy of testing liquid, respectively. Table 3.3 shows the values of polar and dispersive components of surface tension for water and formamide. Using this method, the surface free energy of fibers was calculated and presented in Table 3.4.

Table 3.3

Surface Tension Components of Water and Formamide

Liquid	Polar component ($\boldsymbol{\gamma_l^p}$, mJ/m^2)	Dispersive component ($\boldsymbol{\gamma_l^d}$, mJ/m$^{2)}$
Water	51	21.8
Formamide	19	39

As shown in Table 3.4, the contact angles of the untreated fibers for water and Formamide

were 58.37°, 42.41°. The polar component and the dispersive component of the fiber were 21.04 mJ/m2 and 23.73 mJ/m2, respectively. The total surface free energy was measured as 44.77 mJ/m2. As the Fe content was increased from 0% to 6.8%, 15.9% and 18.0%, the contact angles of water on sample increased from 58.37° to 60.26°, 69.53° and 70.64°, and the contact angles of formamide reduced from 42.41° to 38.63° to 37.78° and to 33.85° accordingly. The two partitions of total surface free energy preformed different trends: the dispersive component increased from 23.73 mJ/m2 to 29.40 mJ/m2, 41.71 mJ/m2 and 47.88 mJ/m2, with the same change of Fe content. However, it was a decrease from 21.04 mJ/m2 to 16.67 mJ/m2, 7.08 mJ/m2 and 5.13 mJ/m2 for the polar component of surface free energy. Also, the total surface free energy increased from 44.77 mJ/m2 to 46.07 mJ/m2, 48.78 mJ/m2 and 53.02 mJ/m2, respectively.

Table 3.4

Surface Free Energy of Kenaf Fibers Before and After Magnetization Treatments

Sample	Fe content	γ_s^p(mJ/m^2)	γ_s^d (mJ/m^2)	γ_{total}(mJ/m^2)
0	0%	21.04	23.73	44.77
1	6.78%	16.67	29.40	46.07
2	15.87%	7.08	41.71	48.78
3	18.02%	5.13	47.88	53.02

The DCA results and the surface free energy calculations shown in Tables 3.2 and 3.3 illustrated that the surface energy increased as the iron content increased. Two parts of changes occurred when the non-polar component increased and the polar component decreased. This can

be explained that the iron oxide crystallization occupied and replaced the functional group on the surface of fibers, weakened the active force between fibers, and reduced the interacting potentials of the fibers surface. However, the polarity of fibers surface increased because of the strong polarity of iron oxide.

3.4 Modulus of Elastic (MOE) for Magnetic Composites

Table 3.5 shows the Modulus of Elasticity (MOE) of the magnetized and un-magnetized composites. As the Fe content increased from 0% to 6.8%, 15.9% and 18.0%, MOE was decreased from 2,875MPa to 2,729MPa, 2,487MPa and 2,007MPa accordingly. Xia et al (2015) reported that, the MOE of the kenaf fiber-unsaturated polyester composites was 4,186 MPa, which was in the same range of these presented results.

The results indicated that as the Fe content increased, the MOE of magnetic kenaf fiber composites decreased. This may be due to the reduction of the adhesion between the kenaf fibers, as the fiber pores were occupied by the crystallization of iron oxide.

Table 3.5

Modulus of Elasticity (MOE) of the Magnetized and Un-Magnetized Composites

Sample	Modulus of Elastic (MPa)	
	Average	St. Div.
0	2,875	445.13
1	2,729	513.60
2	2,487	697.15
3	2,007	375.52

3.5 EM Shielding Effectiveness of Magnetized Fiberboard

Figure 3.2 shows the EM shielding effectiveness of the magnetic fiberboards with different Fe contents. The shielding effectiveness of air with the same thickness of kenaf fiber composites was also measured. It was observed that as the Fe content increased from A (Sample 0, 0%Fe) to B (Sample 1, 6.8%Fe), C (Sample 2, 15.9%Fe) and D (Sample 3, 18.0%Fe), the shielding effectiveness was increased significantly. The percentage of shielding energy under different frequencies changed from 30 - 50% for Sample 0, to 60 - 70% for Sample 1 with 6.8% Fe, 65 - 75% for Sample 2 with 15.9% Fe, and to 75 - 80% for Sample 3 with 18.0% Fe.

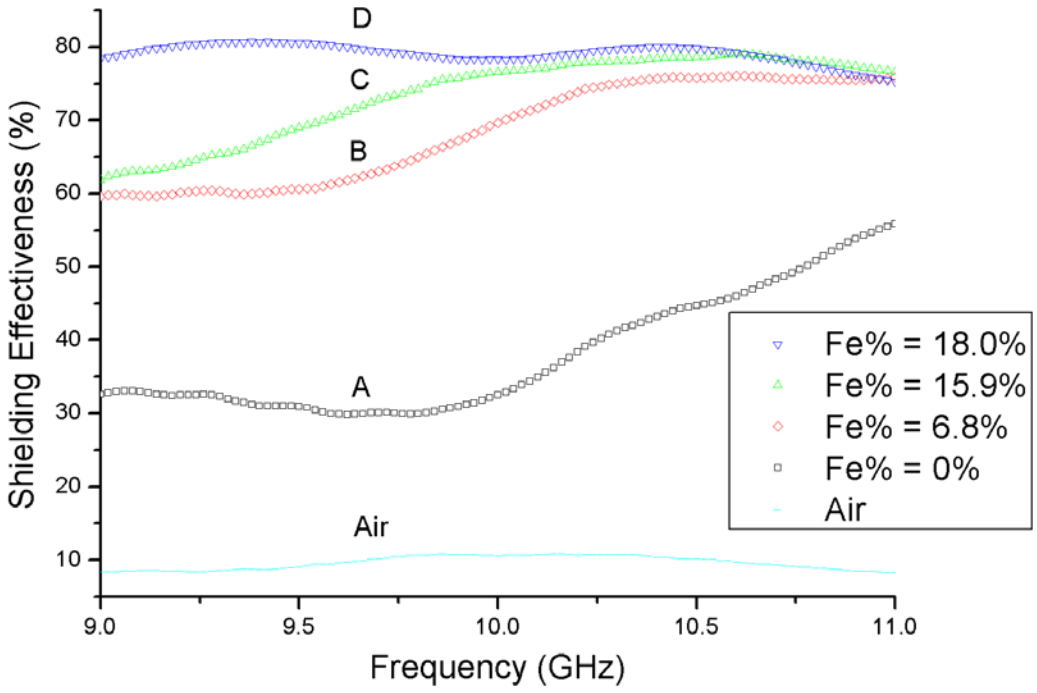

Figure 3.2. EM shielding effectiveness of the magnetized fiberboard with different Fe contents: (A) Sample 0, Fe content=0%, (B) Sample 1, Fe content=6.8%, (C) Sample 2, Fe content=15.9%, (D) Sample 3, Fe content=18.0%.

CHAPTER 4

CONCLUSIONS

I. From the SEM images, the changes of iron oxide nanoparticle amounts were observed. The iron oxide nanoparticles were introduced by the magnetization treatment and deposited to the kenaf fiber surfaces, improved the composite's EM shielding effectiveness.

II. By the incorporation of iron oxide, the total surface free energy increased from 44.8 mJ/m^2 to 46.1 mJ/m^2, 48.8 mJ/m^2 and 53.0 mJ/m^2, as the Fe content increased from 0% to 6.8%, 15.9% and 18.0%, respectively. Although the surface energy was reduced by the magnetizing treatment, the polar component of the surface energy was increased.

III. As the Fe content increased from 0% to 18.0%, the MOE of the fiberboard was reduced about 30% from 2,875 MPa to 2,007 MPa.

IV. The shielding effectiveness of kenaf composites was increased by incorporating iron oxide particles into fibers. As the Fe content increased from 0% to 18.0%, the shielding effectiveness was increased from 30-50% to 75-80%.

REFERENCES

Al-Saleh, M. H., & Sundararaj, U. (2009). Electromagnetic interference shielding mechanisms of CNT/polymer composites. *Carbon*, *47*(7), 1738-1746.

Bollen, P., Quiévy, N., Huynen, I., Bailly, C., Detrembleur, C., Thomassin, J. M., & Pardoen, T. (2013). Multifunctional architectured materials for electromagnetic absorption. *Scripta Materialia*, *68*(1), 50-54.

Dřínovský, J., & Kejik, Z. (2009). Electromagnetic shielding efficiency measurement of composite materials. *Measurement science review*, *9*(4), 109-112.

Hitachi. Instruction Manual for Model S-4800 Field Emission Scanning Electron Microscope.

Hou, C. L., Li, T. H., Zhao, T. K., Liu, H. G., Liu, L. H., & Zhang, W. J. (2013). Electromagnetic wave absorbing properties of multi-wall carbon nanotube/Fe 3 O 4 hybrid materials. *New Carbon Materials*, *28*(3), 184-190.

Huynen, I., Quiévy, N., Bailly, C., Bollen, P., Detrembleur, C., Eggermont, S., ... & Pardoen, T. (2011). Multifunctional hybrids for electromagnetic absorption. *Acta Materialia*, *59*(8), 3255-3266.

Jalali, M., Dauterstedt, S., Michaud, A., & Wuthrich, R. (2011). Electromagnetic shielding of polymer–matrix composites with metallic nanoparticles. *Composites Part B: Engineering*, *42*(6), 1420-1426.

Koh, Y. N., Sambasevam, K. P., Yahya, R., & Phang, S. W. (2013). Improvement of microwave absorption for PAni/HA/TiO2/Fe3O4 nanocomposite after chemical treatment. *Polymer Composites*, *34*(7), 1186-1194.

Kwon, J. H., Park, S. B., Ayrilmis, N., Kim, N. H., & Kwon, S. M. (2013). Electromagnetic interference shielding effectiveness, electrical resistivity and mechanical performance of carbonized medium density fiberboard. *Journal of Composite Materials*, *47*(16), 1951-1958.

Lakshmi, K., John, H., Mathew, K. T., Joseph, R., & George, K. E. (2009). Microwave absorption, reflection and EMI shielding of PU–PANI composite. *Acta Materialia*, *57*(2), 371-375.

Li, X., Yi, H., Zhang, J., Feng, J., Li, F., Xue, D., ... & Mellors, N. J. (2013). Fe3O4–graphene hybrids: nanoscale characterization and their enhanced electromagnetic wave absorption in gigahertz range. *Journal of nanoparticle research*, *15*(3), 1-11.

Li-juan, W., Jian, L., & Yi-xing, L. (2005). Surface characteristics of electroless nickel plated electromagnetic shielding wood veneer. *Journal of Forestry Research*, *16*(3), 233-236.

Nagasawa, C., Kumagai, Y., Urabe, K., & Shinagawa, S. (1999). Electromagnetic shielding particleboard with nickel-plated wood particles. *Journal of Porous Materials*, *6*(3), 247-254.

Saini, P., Choudhary, V., Singh, B. P., Mathur, R. B., & Dhawan, S. K. (2009). Polyaniline–MWCNT nanocomposites for microwave absorption and EMI shielding. *Materials Chemistry and Physics*, *113*(2), 919-926.

Saini, P., Choudhary, V., Singh, B. P., Mathur, R. B., & Dhawan, S. K. (2011). Enhanced microwave absorption behavior of polyaniline-CNT/polystyrene blend in 12.4–18.0 GHz range. *Synthetic Metals*, *161*(15), 1522-1526.

Thermo Cahn Instruments. Dynamic Contact Angle Analyzer Tutorial.

Tong, X. C. (2008). *Advanced materials and design for electromagnetic interference shielding*. CRC Press.

Wang, L. J., Li, J., & Liu, Y. X. (2006). Preparation of electromagnetic shielding wood-metal composite by electroless nickel plating. *Journal of Forestry Research*, *17*(1), 53-56.

Xia, C., Shi, S. Q., Cai, L., & Hua, J. (2015). Property enhancement of kenaf fiber composites by means of vacuum-assisted resin transfer molding (VARTM). *Holzforschung*, *69*(3), 307-312.